applied optics

Self-written waveguides in photopolymer

Ra'ed Malallah,[1,2] Derek Cassidy,[1] Inbarasan Muniraj,[1] James P. Ryle,[1] John J. Healy,[1] and John T. Sheridan[1,*]

[1]School of Electrical and Electronic Engineering, IoE[2] Lab, College of Engineering and Architecture, University College Dublin, Belfield, Dublin 4, Ireland
[2]Physics Department, Faculty of Science, University of Basrah, Garmat Ali, Basrah, Iraq
*Corresponding author: john.sheridan@ucd.ie

Received 3 April 2018; revised 25 May 2018; accepted 28 May 2018; posted 31 May 2018 (Doc. ID 327456); published 26 June 2018

Self-written waveguide (SWW) trajectories fabricated inside a dry photopolymer bulk material, acrylamide/polyvinyl alcohol (AA/PVA), are studied. Their production using both Gaussian and Laguerre–Gauss exposing (writing) light beams, output from optical fibers, is explored. The formation of the primary and secondary eyes is also discussed. Furthermore, the interactions that take place when two counterpropagating beams pass through the photopolymer material (both Gaussian and Laguerre–Gauss) are examined. In all cases experimental and theoretical results are presented. Good agreement between the predictions of the proposed model and experimental observations are demonstrated.

OCIS codes: (160.5470) Polymers; (260.5950) Self-focusing; (250.5460) Polymer waveguides; (160.5335) Photosensitive materials; (130.4310) Nonlinear; (070.2575) Fractional Fourier transforms.

https://doi.org/10.1364/AO.57.000E80

1. INTRODUCTION

Optical self-written waveguides (SWWs) have been demonstrated in various photopolymerizable materials [1–4]. The diffraction of propagating waves in such materials can be effectively compensated during SWW formation. A phenomenological model [3,5–7], can be used to describe the refractive index change taking place in such materials. In this paper, attempts to further extend the potential uses of photopolymer material for SWW fabrication are presented.

The photopolymer material acrylamide/polyvinyl alcohol (AA/PVA) is used throughout this paper. A detailed description of the preparation of the AA/PVA photopolymer used here was presented in [8]. Optically induced growth of SWWs in such a free radical photopolymerization system is discussed. The effects of the optical beam absorption (due to the presence of photosensitizer) and the self-modulation due to waveguide formation are shown to alternately dominate the SWW process at different times (during the exposure).

There is an ever-increasing demand for optical waveguides. This is in part driven by the desire to implement integrated optical circuits and devices. Such devices find wide use in optical sensing and optical telecommunication applications [9,10].

There are several ways to generate optical waveguides. As indicated, the method discussed here involves exposing a photosensitive self-developing material using a spatially localized beam at the input of the material surface. As a result, photopolymerization takes place, increasing the local refractive index within the material. The exposing light is absorbed as part of the writing process. The way in which the light is absorbed affects SWW formation. In such materials, dye excitation due to absorption generates the radicals necessary for polymer chains to start growing [11]. As a consequence of SWW formation, the exposing laser beam becomes self-trapped along the input propagation axis in the material volume [12,13]. This self-writing process has been applied to provide solutions for many practical problems, such as to create connections between optical fibers and microtips at the end of optical fibers, generate biologically inspired microstructures, and implement strain sensors [1,3].

Exposing the photopolymerizable materials requires use of light of a suitable wavelength. This wavelength depends on the choice of an appropriate dye sensitizer. The dye type and dye concentration chosen will depend on the self-writing mechanism, the application, and the details of the experimental setup and procedures used.

In this paper, the model used to predict the SWW recording process is briefly described [3]. The predictions of this model are then compared to the experimental results presented. The objective here is to investigate the use of both Gaussian and Laguerre–Gauss (LG) light beams to from SWWs.

Both Gaussian and LG shaped modes are described in some detail in [14]. LG beams can be used to transfer orbital momentum to trapped particles, inducing them to rotate around the optical axis. LG modes are interesting examples of higher-order beams which can be conveniently described. Several other potential applications of LG modes in telecommunications are also emerging. The theoretical description of the electric field of a LG mode is given in [14–16]. One way of expressing the LG mode is

$$u^{\mathrm{LG}} = \sqrt{\frac{2}{\pi\omega^2(z)}}\exp\left[-\frac{r^2}{\omega^2(z)}\right]\exp\left[-i\left(\frac{kr^2}{2R(z)}\right)-\tan^{-1}\left(\frac{z}{b}\right)\right], \quad (1)$$

where r is the radial distance from the center axis of the beam, and $k = 2\pi/\lambda$. $\omega(z)$ is radius at which the field amplitudes fall to $1/e$ of their axial values (i.e., where the intensity value fall to $1/e^2$ of the axial $r = 0$ value). $R(z)$ is the radius of the beam, that is, the radius of curvature of the beam's wavefronts along z. b is the Rayleigh range [15,16].

As noted, both Gaussian and LG light beams are used during the experimental generation of the SWWs presented here. The resulting photosensitive response and subsequent waveguide evolution is experimentally observed during SWWs formation in dry AA/PVA bulk samples [2,3,8]. Numerical simulations corresponding to these experiments are carried out [3]. The resulting predictions are used to develop further understanding of the role of the material response during the self-writing process.

2. SWWs MODELLING

Photopolymer materials undergo several photochemical reactions (depending on the photosensitizer used) when illuminated by appropriate light. The photopolymerization process that occurs in AA/PVA material is free-radical polymerization [17]. During the photochemical process, there are four main reactive phases: (1) initiation, (22) propagation, (3) termination, and (4) inhibition [18]. In this study, a dynamically induced three-dimensional (3D) photopolymer distribution is formed, with an incident beam propagating along the z axis, perpendicularly illuminating a cross sectional area in the x-y plane. In order to create a permanent SWW, a saturatable solid photosensitive material is used, as stable, long-lasting refractive index changes take place in response to exposure at a specific wavelength [19].

The photopolymers discussed are essentially made up of a monomer (AA), binder (PVA), cross-linker [bisacrylamide, (BA)], electron donor [triethanolamine (TEA)] and dye [Eosin-Yellowish (EY)]. When the photopolymer material is exposed, the ground state dye absorbs light and becomes excited, and this process leads to the generation of monomer radicals. These monomer radicals result in the initiation of growing polymer chains (as the monomer combines) [20]. The light absorption process is fundamentally dynamic and nonlinear in nature. The incoming light intensity is proportional to the square of the amplitude of the incident electric field, $I = |E^2|$. The resulting polymer chains are formed in the cylindrical volume along the path of the light beam, that is, along the z axis, leading to the waveguide having different refractive index variations in x, y, and z. Control of the refractive index formed, and hence of the shape of the SWWs, has previously been studied [21,22]. Focused Gaussian intensity profile exposing beams were examined in most previous cases.

A rate equation for the ground state photosensitizer concentration, $[A(x,y,z,t)]$ (mol cm^{-3}), which is expressed as a function of the material sample space (x,y,z) and exposure time t, is given by [12,13]

$$\frac{\partial[A(x,y,z,t)]}{\partial t} = -k_a(x,y,z,t)[A(x,y,z,t)]. \quad (2)$$

This equation predicts the variation of $[A(x,y,z,t)]$ (mol cm^{-3}) given that the rate of production of the excited state photosensitizer is $k_a(x,y,z,t)(s^{-1})$. We note that this rate also depends on the exposing beam intensity, namely, $k_a(I)(s^{-1})$ [3]. In order to predict the "shape" (refractive index and path) of the SWW formed in the bulk sample, the refractive index and absorptivity are initially assumed to be uniform throughout the material. Optical field propagation inside the material is assumed to be governed by the paraxial wave equation [2,12,13]

$$\frac{\partial^2 E}{\partial z^2} + 2ik_0 n_0\frac{\partial E}{\partial z} + \nabla_\perp^2 E + 2k_0^2 n_0 \Delta n E + 2k_0^2\Delta n^2 E + ik_0 n_0 \alpha E = 0, \quad (3)$$

where E is the amplitude of the scalar electric field, and z is the propagation direction. n_0 is the average refractive index, and $k_0 = 2\pi/\lambda$ is the wave number inside the homogenous medium. In Eq. (3), $\nabla_\perp^2 = \partial^2/\partial x^2 + \partial^2/\partial y^2$ denotes the 2D Laplace operator.

The optically induced refractive index change is denoted by Δn, and the absorption parameter is given by α. To describe the refractive index change induced in the material, $\Delta n(x,y,z,t)$, a simple model, commonly used in the literature, is applied to describe the effects of photopolymerization. The evolving change in refractive index, which is in a constant state of change during the self-writing process, is assumed to satisfy [12,13]

$$\frac{\partial\Delta n(x,y,z,t)}{\partial t} = AI^p(x,y,z,t)\left(1-\frac{\Delta n(x,y,z,t)}{\Delta n_s}\right), \quad (4)$$

where Δn_s is the fixed (maximum) saturation value of the refractive index change, and $I(x,y,z,t)$ is the local optical exposing intensity. The coefficient A is a real coefficient (not a concentration $[A]$) that depends on the material properties, and p represents a number of photons. For the photopolymerization process discussed here, it is assumed that $p = 1$ [6,7].

3. EXPERIMENTAL SETUP

The experimental system used to perform the work discussed here is shown in Fig. 1. As can be seen, two microscopic objective lenses, (1) and (2), are used to couple a laser beam source [532 nm, 0.5 mW) which is measured from the output end of each fiber optic cable (FOC)] into two different FOCs.

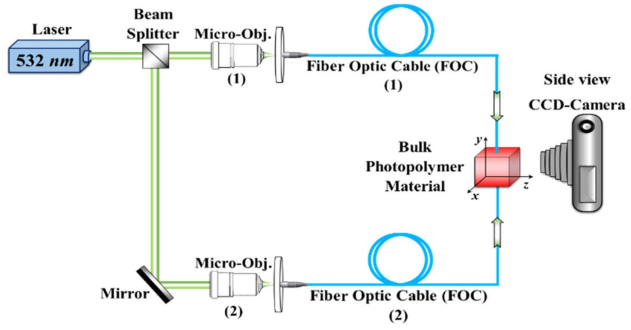

Fig. 1. Schematic diagram of the setup used to monitor SWW formation using two FOCs.

The output beams are shown simultaneously illuminating the front/back faces of the photopolymer bulk material. A charge-coupled device (CCD-Camera) is used to detect the generation of the waveguiding structures from the side. In fact, using the setup in Fig. 1, light can illuminate the bulk material from either side separately or simultaneously.

The shape of the exposing beams which are studied in this paper) depends on the type of FOCs used; for instance, if single mode (SM) optical fibers are used, the exposing beam is Gaussian in shape. During exposure the ends (tips) of the FOCs are placed in contact with the sample surface; no index matching is used.

4. EXPERIMENTAL AND NUMERICAL RESULTS

The preparation of the photopolymer bulk material samples has previously been presented in detail in [8]. In the photopolymer used here, EY is the photosensitizer, where the initial photosensitizer concentration used is 1.22×10^{-7} mol cm^{-3} [3,8]. In order to gain a better understanding of the reactions of these dyes, the UV–visible absorption spectra of an AA/PVA solution that included EY was examined; see Fig. 2. The spectrum was acquired using a double beam (Jasco V-650) spectrophotometer. The measured absorption spectrum in the visible range is shown. The absorption of the material was obtained by measuring the attenuation of light intensity as a beam passed through the material; that is, the device measured the amount of light absorbed as it passed through the material. As can be seen from Fig. 2, the material that has been prepared is most sensitive (absorbance maxima) in the green at $\lambda = 523$ nm. Furthermore, the photoluminance intensity is greatest (emission maxima) at the longer wavelength of $\lambda = 552$ nm [23,24]. We note that some of the light imaged by the camera shown in Fig. 1 will be such emitted light.

A. SWW Using a Single Gaussian Light Beam

Light from SM fibers is first used to expose the sample. Figure 3 illustrates the intensity profile of a normalization Gaussian light beam intensity input into the photopolymer material using a single mode FOC. The highest optical power is in the center of the optical beam.

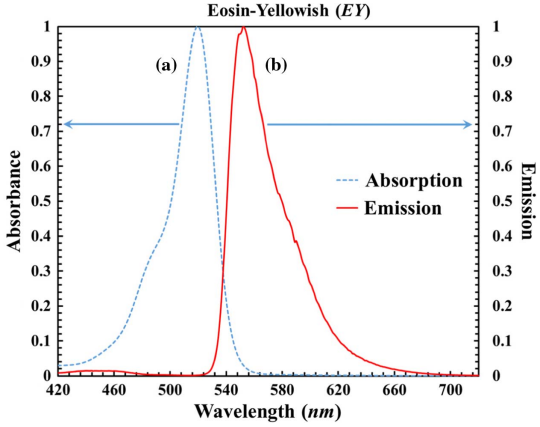

Fig. 2. Normalized (a) absorbance (blue dashed curve) and (b) emission (red curve) spectra plotted against wavelength for AA/PVA photopolymer material including EY.

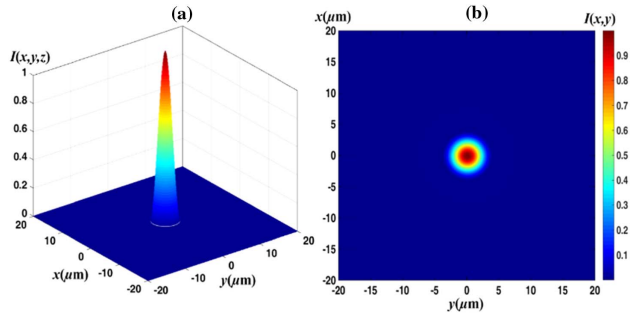

Fig. 3. Illustration of an ideal normalization Gaussian light beam intensity: (a) 3D side view and (b) 2D top view (contour plot).

This means that most absorption (and the highest rate of photopolymerization during illumination) will take place along this central region in x and y. The form of the LG beam is discussed later (see Fig. 8).

This intensity distribution is incident on the bulk photopolymer material. The light beam output from an optical fiber cable into a homogenous passive medium will expand as it propagates through the medium. However, inside the photopolymer the light beam begins to focus because of the increasing localized cross sectional refractive index profile (due to the polymerization process).

In this study the SWWs are produced inside solid photopolymer. The SWWs formed when using two incident exposing beam shapes are studied: (1) using a simple mode (Gaussian light beam), and (2) using a higher order mode (LG beam). In our experiments, these beam shapes are generated using appropriate inputs to excite such modes in optical fiber cables.

First, such a single Gaussian light beam is used to produce a single channel waveguide in a photopolymer media. In Fig. 4, a comparison between the experimental results and the predictions of the model (for the exposure time $t_{\text{exp}} = 1200$ s and power intensity $P_0 = 0.5$ mW), is presented. The SM fiber patch cable (ThorLabs, P1-460B-FC-5) is used to create a single channel (SWW) under dark room conditions. The fiber end is placed directly in contact with the input face ($z = 0$) of the dry bulk AA/PVA sample, no index matching being used.

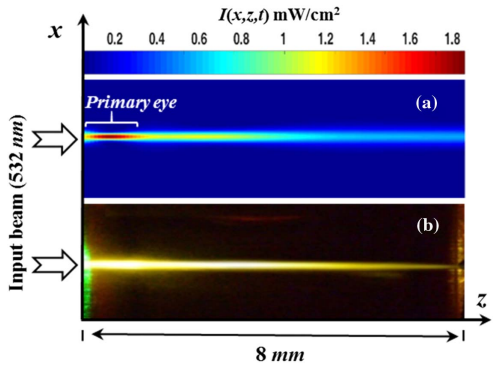

Fig. 4. SWW formation in photopolymer material: (a) theoretical prediction $I(x, z, t)$mW/cm^2; and (b) experimental image captured when $t_{\text{exp}} = 1200$ s and $P_0 = 0.5$ mW (total power in one input beam).

The CCD (Nikon D3200, DX 18–55 mm 1:3.5-5.6 G VR, 10× microlens 52 mm) captures a side view image and is focused to image the SWW formed inside the material. In this way the propagation of the beam through the sample and the generation of the waveguide structures are monitored [2].

The camera (placed to capture a top/side view of the sample; see Fig. 1) images the light scattered (emitted) toward the camera during SWW formation. The recorded intensity images are compared with the corresponding numerical simulations, that is, the predicted 2D cross sectional intensities along the SWW, $I(x,z,t)\text{mW/cm}^2$. It is assumed that the light imaged by the camera is closely related to the intensity present along the SWW, that is, it is proportional to $I(x,y,z,t)$.

Exposure leads to an increase of the refractive index during photopolymerization. Therefore, a lensing effect is created near the front face (input side) of the material. This acts to focus the input light and creates a "primary eye" [6]; see Fig. 4(a). The position of this high intensity focal point moves along the z axis with time. This behavior, shown in Fig. 4(a), is observed in the sequence of experimental images (captured by CCD), one is shown in Fig. 4(b).

The resulting SWW structures are stable. To emphasize this point, one of our SWW channels formed inside an AA/PVA sample was (post-exposure) stored under dark room conditions, at an average temperature of ~20°C and a relative humidity of ~40%, for a year. It was then re-examined using the experimental setup shown in Fig. 1. The SWW still functioned and could be seen. No obvious degradation was observable.

In order to produce Fig. 4(b), the images of the sample were captured under fluorescent room lighting. In general, it has been found that no precautions were needed to protect the waveguide from the effects of the environment under normal laboratory working conditions, namely, oxygen, humidity, and exposure to broadband ambient lighting (certainly for a short period of time) [2]. We note that this is very different from the case when AA/PVA material layers are used for holography studies. In those cases, if unsealed, that is, uncover-plated, the material can react strongly (and adversely) to environmental conditions post-exposure [2,23–26]. As noted, a special sample preparation procedure is used here compared to that used to make the much thinner and softer holographic layers.

When the exposing light intensity (i.e., output from the FOC) is increased to $P_0 = 1.0$ mW, "secondary eyes" begin to be observed; see Fig. 5. Index changes occur more rapidly when the exposing intensity is increased. Initially, the most rapid refractive index increases occur at the input face and along

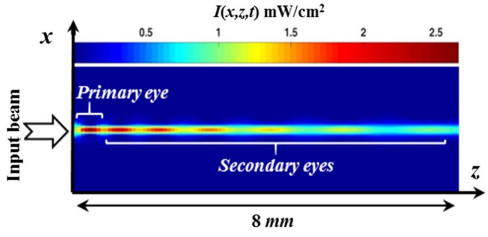

Fig. 5. Numerical simulation for SWW formation in photopolymer material. A single input Gaussian beam is used. $t_{exp} = 1200$ s, $P_0 = 1.0$ mW.

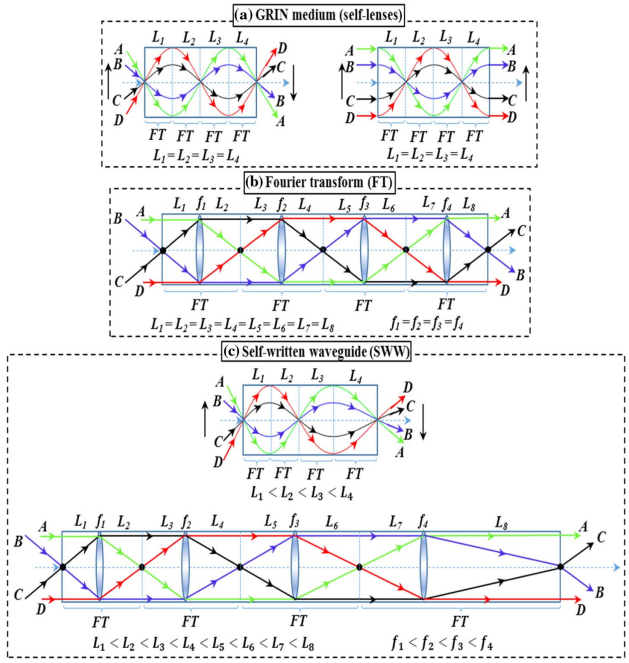

Fig. 6. Scheme of light propagations as (a) GRIN, (b) Fourier transform, and (c) SWW.

the propagation axis. As the process proceeds, the cross-sectional index change gradually grows in x, y, and also along z.

Effectively, over time more lenses in series, having different focal lengths, are generated along the SWW. This occurs as part of the waveguide channel formation process. It is worth noting that the distances between the eyes (lens focal points), shown in Fig. 5, are different because of the SWW formation process arising from the nonlinearity of the material response.

Thus, the eyes arise due to light propagation along an evolving quadratic cross-sectional index profile waveguide. This is similar to the effect of a selfoc lens or graded index (GRIN) medium, see Fig. 6(a). This can be appreciated using the optical Fourier transform (FT), see Fig. 6(b). GRIN medium are fabricated having a quadratically varying refractive index profile across their cross section. The cross-sectional profile does not change with z. Light rays propagate along sinusoidal path trajectories as they move through the medium. In a long GRIN medium, the rays periodically refocus (cross over one another); see Fig. 6(c). Over a specific length of GRIN medium, $4L$, the input field repeats, as in the action of an idealized imaging system. This is equivalent to the sequential applications of four FTs. Over a distance of $2L$, the input field appears at the output upside down (inverted). The FT of the input field appears at the output after propagating a GRIN length of L, and this effect is used to collimate light from point sources. In Fig. 6(b), L indicates the periodic displacement between lenses along the light path. Examining the results in Fig. 5 indicates that the SWW acts like a stretched or elongated GRIN lens.

B. Materials and Reactions

Our dry AA/PVA samples contain the following components: a binder (PVA), a monomer (AA), a cross-linker (BA), and an electron donor (TEA). For the specific material under examination

here, EY dye is used to sensitize it in the green, namely, at $\lambda = 532$ nm [23,25], where the initial photosensitizer concentration used is 1.22×10^{-7} mol cm^{-3} [3,8]. However, in contrast to holographic material preparation, both heating and vacuum cooling are employed to produce rugged (highly dense) bulk samples [2,7].

Let us briefly describe the processes taking place during free radical photopolymerization [2,17,23–30]. First, under the influence of light of suitable wavelength ($\lambda = 532$ nm), the ground state dye molecule (EY) absorbs a photon and is promoted into its excited singlet state. The resulting singlet state dye molecule can undergo intersystem crossing into the longer lived (more stable) triplet state [23,25]. The reaction between the excited triplet state dye and the electron donor (TEA) leads to the production of initiator/primary radicals, which can react with the monomers (AA) and cross-linkers (BA) to produced chain initiators [17]. The chain initiator can attach itself to another monomer molecule by addition to the monomer C═C bond, yielding a growing polymer radical with an active tip, that is, once the monomer is polymerized [31]. Termination can happen by either disproportionation or combination, both of which involve two growing macroradicals interacting to stop growth [17,30]. Inhibitors are chemicals (e.g., oxygen) which react with the initiating and propagating radical species to rapidly remove (scavenge) such radicals [29]. The photochemical processes taking place during free radical polymerization produce long polymer chains. The resulting polymer can have a significantly higher refractive index than the original monomer. In the case of AA/PVA, the refractive index of the polymer is $n_p = 1.52$, while that of the AA monomer is $n_m = 1.46$ [2,27,28].

As noted, extensive studies applying AA/PVA photopolymer layers to produce volume holographic gratings have been reported [23,25]. In such cases, the AA/PVA photopolymer was prepared as a thin dry film, typically 50–150 μm thick [28,29,32]. The holographic studies indicate that self-processing photopolymers have many useful properties [17,23–30]. These include reasonable (1) refractive index change (modulation), (2) sensitivity, (3) spatial homogeneity, (4) grating lifetime, and (5) cost. AA/PVA is an interesting research material.

When the material is prepared as a thin planar layer (i.e., an optically thick layer), for use in recording volume holographic gratings [28,29,32], the resulting layers have a relatively large surface area to volume ratio and contain appreciable amounts of oxygen and moisture. Sealing (cover-plating) is necessary to reduce inhibition effects [33–35]. Excess monomer in the layer can lead to the monomer molecules (pre- and post-exposure) crystallizing at the layer surface, where they absorb moisture from the air and redissolve, yielding an undesirable a sweating process [25,32]. Previously, such material processes have been observed in our laboratory and result in the appearance of clearly visible surface contamination pre-exposure. In contrast to such thin planar geometry layers, specially prepared bulk samples are used here [2]. The self-written waveguides reported are completely sealed deep inside the solid bulk volume. Furthermore, no surface contaminants have been observed either pre- or post-exposure.

C. Counterpropagation of Two Gaussian Light Beams

Next, we examine the case involving two simultaneous exposures using two Gaussian beams input from optical fibers positioned at either side of the sample; see Fig. 1. Prior to exposure, the fibers are aligned (along the z axis) using a microscope. The two inputs are separated by 8 mm (the material samples) aligned along the same line (z-axis). A series of experimental images captured at different exposure times is shown in Fig. 7, (right hand column). The corresponding numerical simulations are presented on the left-hand side of Fig. 7. The predictions are in good qualitative agreement with the experimental results.

Initially in Fig. 7, greater spreading of the input beam propagation during the writing process ($t_{\text{exp}} = 50$ s) is observed. Subsequently, as the exposure continues ($t_{\text{exp}} = 100$, 200, 300, and 600 s), enhanced confinement (self-trapping) of the beam is observed. This investigation, using counterpropagating Gaussian beams, demonstrates that a continuous confining structure is eventually created. The resulting SWW can be used to guide light between the two FOCs along a specific path (trajectory).

It might be thought that use of two mutually coherent exposing beams during exposure might lead to the recording of an unslanted reflection geometry grating. Such a grating is not observed, and we note that (1) the period of such a grating could be very small $\lambda/2n_A \sim 180$ nm, and (2), as will be indicated, the material appears to act to reduce beam coherence (see Fig. 11).

Previously, SWW fabrication processes for creating sensors and coupling structures between two optical fibers have been reported [36,37]. Previously we have demonstrated the possibility of coupling two optical fibers with two SWWs formed by counterpropagating beams. Results for four exposures of different durations are presented. The simulations in Fig. 7 predict the confinement of the two optical beams as they propagate toward one another. Once the SWWs begin to form, the induced changes in the refractive index start to compensate for the diffractive spreading [3,26]. In Fig. 7 the arrows indicate the direction of the two counterpropagation beams, input at the

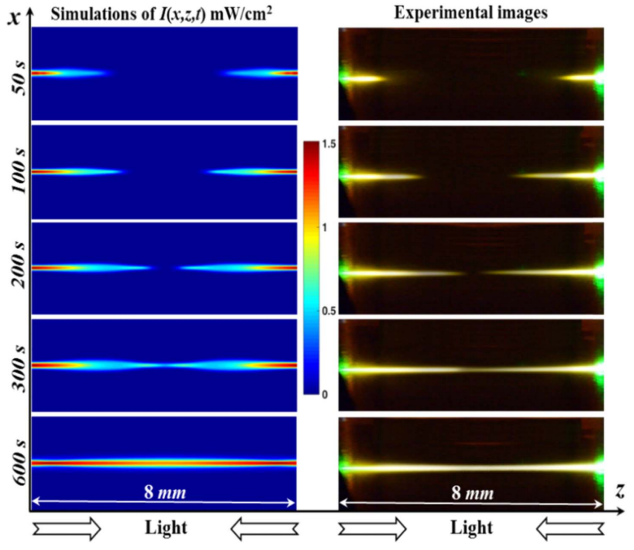

Fig. 7. Interactions of two counterpropagating Gaussian beams forming SWW in photopolymer material using $P_0 = 0.5$ mW (i.e., the output from each FOC is 0.5 mW). Exposed for five different durations, $t_{\text{exp}} = 50$, 100, 200, 300, and 600 s. The corresponding simulations (left) and experimental results (right) are shown.

opposite sides of the sample, separated by 8 mm. The two optical beams crossing one another might be expected to interfere; however, based on the results of our holographic studies, the material's spatial frequency response does not allow such fine reflection gratings to be recorded (the response is negligible above 5000 lines/mm), [8].

The joining together of the two channels/waveguides growing from either side has previously been demonstrated [38,39]. The conversion of monomer into polymer produces interaction between the SWWs formed by the counterpropagating beams. The potential practical value of such a technique, for use in splicing (coupling) optical fibers *is situ*, appears high. Importantly, this is achieved without the need to position the FOCs, that is, to perform the high precision mechanical alignment typically required in conventional FOC fusion splicing. Such alignment is difficult between SM fibers for applications within the area of telecommunication [11,40]. The core of such fibers is typically 8–10 μm in diameter. All six degrees of mechanical freedom must be controlled during splicing.

D. SWW Using a Single LG Light Beam

To further explore the possible applications of the self-writing process in this material, SWWs formed when exposing using a LG profile mode (LG_{20}) are examined. Figure 8 shows the normalized optical beam intensity of a LG mode (LG_{20}) [41,42]. In this a case, the light intensity is distributed as a circular (annular) ring around a dark region in the beam center [43,44]. The intensity of this beam is therefore circularly symmetric.

Certain types of laser beams known as vortex beams can be described as LG beams [14,15,43,44]. In such cases, the light wave's phase front twists about (around) the direction of propagation. This twisting of the phase front take place in a spiral fashion while the field has a doughnut-like ring intensity profile [14,45].

When such a beam propagates in free space, the diameter of the ring typically expands due to diffraction. As discussed subsequently, such an optical beam can propagate through our photopolymer medium without changing its annular beam shape (structure), and in the process it forms a doughnut-shaped SWW. While the beam radius may vary, the shape is preserved.

An LG mode, output from an FOC, is incident on the front face of a photopolymer sample (no index matching is used). For this experiment, a multimode Ocean Optics, QBIF200-VIS-NIR optical fiber is used to produce the LG_{20} mode, using the experimental setup illustrated in Fig. 1. In general, to generate the LG

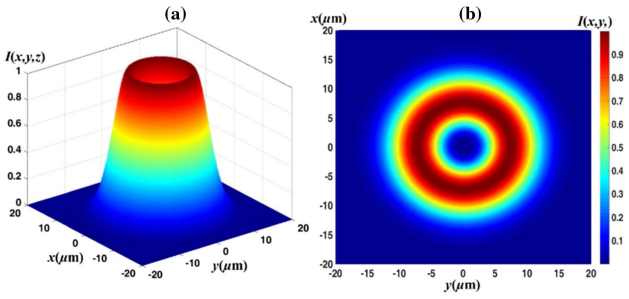

Fig. 8. (a) 3D side view and (b) 2D top view (counter plot) of the normalization of light intensity of a LG mode (LG_{20}), which can be excited and output from a multimode optical fiber cable. The annular cross-sectional beams profile is shown.

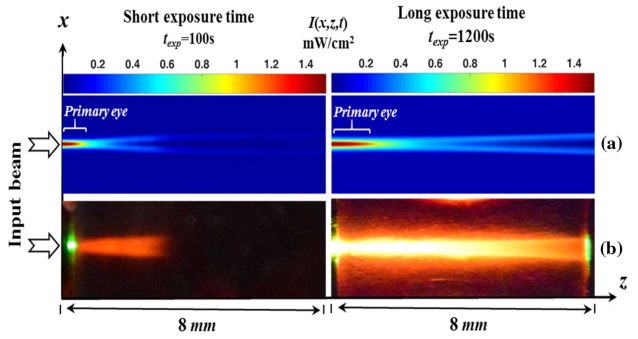

Fig. 9. Effects of LG_{20} mode beam on the formation of the SWWs for both short (t_{exp} = 100 s) and long (t_{exp} = 1200 s) exposure times. (a) Theoretical predictions and (b) corresponding experimental results.

mode, the light input into the FOC is incident at a specific angle with respect to the input core face. This results in strong coupling into the desired LG_{20} mode.

In Fig. 9, side views of the predicted intensity (top) and experimental images (bottom) of the SWW channels formed when a single LG_{20} beam is input are shown. The results indicate that the light beam propagates inside the material and creates a waveguide while keeping the annular beam structure unchanged. However, the diameter of the beam (and SWW) does change in crossing the material. Examining Fig. 9, it can be seen that the observed (experimental) results are in good qualitative agreement with the numerical simulations, once again confirming the reasonableness of our model and of the material parameter values used to simulate these results. No change in the structure of the beam or of the resulting waveguide are observed (i.e., no beam self-cleanup; see [46]). Therefore, the input LG_{20} mode is not converted into a Gaussian mode shaped output beam. Furthermore, there is no bending of the LG_{20} beam trajectory away from the z axis during SWW fabrication.

The location of highest intensity, that is, the primary eye, appears close to the front face of the material sample; see Fig. 9. This indicates that lensing action is taking place due to photopolymerization based index changes.

In Fig. 10 the predicted cross-sectional beam intensity has been plotted at the depths when t_{exp} = 1200 s. We note that

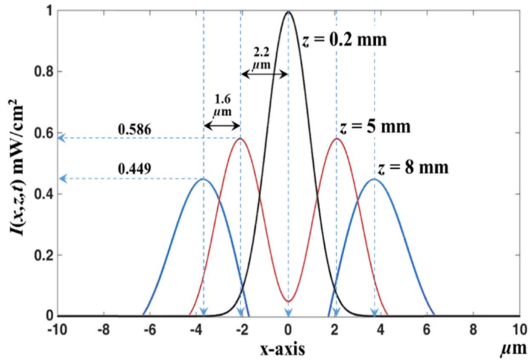

Fig. 10. Predicted normalized cross-sectional beam profile inside the material at three different depths (0.2, 5, and 8 mm) when t_{exp} = 1200 s.

when $z = 0.2$ mm, the beam is predicted to have a cross-sectional Gaussian profile (in the figure, normalization is with respect to this maximum value).

At $z = 5$ mm, an LG_{20} mode shape is predicted, expanded (in diameter) and attenuated (0.586 mW/cm^2). Finally, Fig. 10 also shows the predicted output beam ($z = 8$ mm) when $t_{exp} = 1200$ s. At the output the LG_{20} mode contained is wider and has a lower maximum value, namely, 0.449 mW/cm^2. The $z = 5$ mm and $z = 8$ mm results are normalized with respect to the maximum value of the predicted beam at $z = 0.2$ mm. As noted, the beam radius expands, with the peaks being located at radial distances of 2.2 and 3.8 μm from the central x axis, when at $z = 5$ and 8 mm, respectively.

In Fig. 11 the measured (a) input and (b) output beam intensity distributions are presented. Both images were captured by a camera placed in the far field. The essential annular structure of the beam has not changed following the SWW process.

In Fig. 11(b) the existence of filaments (filamentation) around the output beam edges is indicated. The observation of filaments indicates that some breaking up of the channel guide has occurred due to the high power of the self-trapped light [2].

Furthermore, while a significant speckle pattern can be observed in the input beam image, see Fig. 11(a), it is greatly reduced in the observed output beam, see Fig. 11(b). Therefore, while the input beam is spatially coherent, the output beam appears to have reduced spatial coherence. The dynamical effects, namely, filamentation and rogue waves, arising when self-processing materials are exposed by speckle is a topic of some interest and has previously been discussed [47].

Figure 11 supports our conclusion that there is no self-bending or self-cleanup of the beam during the polymerization process. For the cases examined, the uniform intensity around the annular incident beam ensures circularly symmetric index changes during formation. In conclusion, the beam appears to retain its mode structure during SWW creation.

E. Counterpropagation of Two LG Light Beams

Finally, work was performed to demonstrate the ability to form SWWs using simultaneous exposure from two optical fibers. The results for two counterpropagating LG modes (LG_{20}) are examined in Fig. 12.

The predicted cross-sectional intensity between the two beams is shown in Fig. 12(a). The corresponding experimental

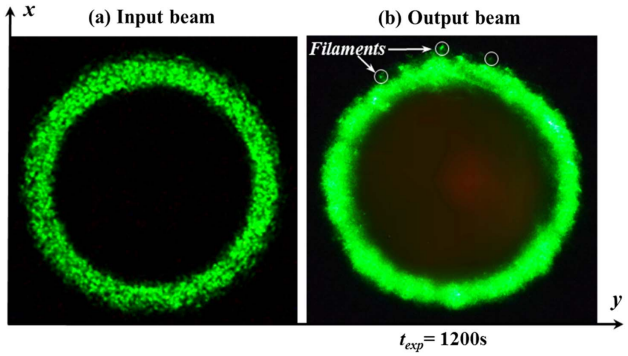

Fig. 11. Experimentally observed (a) input (exposing) and (b) output LG mode beam, imaged in the far field when $t_{exp} = 1200$ s.

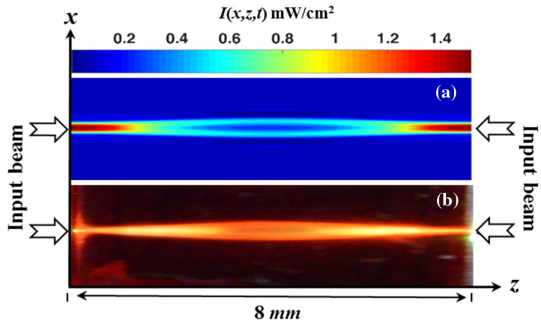

Fig. 12. Two simultaneously counterpropagating LG_{20} mode beams when $t_{exp} = 600$ s and $P_0 = 0.5$ mW (i.e., the output from each FOC is 0.5 mW): (a) numerical simulation, (b) experimental image.

image for this situation is presented in Fig. 12(b) when $t_{exp} = 600$ s. Good qualitative agreement between the experimental result and the corresponding theoretical predictions can be seen.

These results demonstrate the possibility of self-writing different types of connections between optical fiber cables. In this case, two LG_{20} mode carrying optical fiber cables are connected without the alignment process required for conventional fusion splicing.

5. CONCLUSIONS

SWWs may offer a way to address the challenge of fabricating optical interconnects. In this paper it is demonstrated that optical waveguide self-writing is a potentially useful technique for the direct fabrication of aligned guiding structures. Given suitable conditions, the method is capable of being used to repair defective optical connections (waveguides) in sensor or communication networks [10]. It also seems to provide a technique to write specialist mode connections, create GRIN like media (i.e., exhibiting selfoc type behavior), and vary beam spatial coherence [48].

This paper presents a description and comparison of the use of Gaussian and LG modes [14] to write SWWs in AA/PVA material. When modelling light propagation, electromagnetic wave equations assuming the paraxial approximation are used. Results for both single beams and counterpropagating beams are examined.

The model describing the nonlinear photoabsorptive effects taking place during the photoinitiation processes is discussed. Such effects must be included to account for the excitation of the photoinitiator and the associated absorption during photopolymerization throughout the material.

Simulations for both Gaussian (SM fiber) and LG beams (multimode fiber) are performed. Corresponding experimental results are presented and compared to the predictions. Waveguide production is demonstrated, and the results are discussed. A dry, specially prepared bulk photopolymer material of thickness 8 mm is used. The refractive index change formed is clearly sufficient to overcome the diffraction effects; see also [2,3].

Then experimental and theoretical results for SWWs formed when two aligned Gaussian beams counterpropagate simultaneously inside the photopolymer material are examined

for different exposure times. The counterpropagating beams produce a single waveguide. Then the formation of the SWWs arising due to simultaneous exposure by two counterpropagating LG beams is also examined. It is shown that the LG beam profile is preserved. Good qualitative agreement between theory and experiment is found.

These results are very encouraging and provided new insights into the SWW formation process.

Funding. Ministry of Higher Education and Scientific Research (MOHESR); Science Foundation Ireland (SFI); Irish Research Council for Science, Engineering and Technology (IRCSET); Enterprise Ireland.

REFERENCES

1. K. Dorkenoo, O. Crégut, L. Mager, F. Gillot, C. Carre, and A. Fort, "Quasi-solitonic behaviour of self-written waveguides created by photopolymerization," Opt. Lett. **27**, 1782–1784 (2002).
2. H. Li, Y. Qi, J. P. Ryle, and J. T. Sheridan, "Self-written waveguides in a dry acrylamide/polyvinyl alcohol photopolymer material," Appl. Opt. **53**, 8086–8094 (2014).
3. H. Li, Y. Qi, R. Malallah, and J. T. Sheridan, "Modeling the nonlinear photoabsorptive behavior during self-written waveguide formation in a photopolymer," J. Opt. Soc. Am. B **32**, 912–922 (2015).
4. H. Li, Y. Qi, R. Malallah, J. P. Ryle, and J. T. Sheridan, "Self-trapping of optical beams in a self-written channel in a solid bulk photopolymer material," Proc. SPIE **9508**, 95080F (2015).
5. A. S. Kewitsch and A. Yariv, "Nonlinear optical properties of photoresists for projection lithography," Appl. Phys. Lett. **68**, 455–457 (1996).
6. T. M. Monro, L. Poladian, and C. M. Sterke, "Analysis of self-written waveguides in photopolymers and photosensitive materials," Phys. Rev. E **57**, 1104–1113 (1998).
7. T. M. Monro, D. Moss, M. Bazylenko, C. M. Sterke, and L. Poladian, "Observation of self-trapping of light in a self-written channel in a photosensitive glass," Phys. Rev. Lett. **80**, 4072–4075 (1998).
8. R. Malallah, H. Li, D. P. Kelly, and J. T. Sheridan, "A review of hologram storage and self-written waveguides formation in photopolymer media," Polymers **9**, 337 (2017).
9. R. V. Ramaswamy and R. Srivastava, "Ion-exchanged glass waveguides: a review," J. Lightwave Technol. **6**, 984–1002 (1988).
10. A. Günther, A. B. Petermann, U. Gleissner, T. Hanemann, E. Reithmeier, M. Rahlves, M. Meinhardt-Wollweber, U. Morgner, and B. Roth, "Cladded self-written multimode step-index waveguides using a one-polymer approach," Opt. Lett. **40**, 1830–1833 (2015).
11. A. M. Ljungström and T. M. Monro, "Light-induced self-writing effects in bulk chalcogenide glass," J. Lightwave Technol. **20**, 78–85 (2002).
12. A. S. Kewitsch and A. Yariv, "Self-focusing and self-trapping of optical beams upon photopolymerization," Opt. Lett. **21**, 24–26 (1996).
13. A. Anderson and K. Peters, "Finite element simulation of self-writing waveguide formation through photo-polymerization," J. Lightwave Technol. **27**, 5529–5536 (2009).
14. F. Pampaloni and J. Enderlein, "Gaussian, Hermite-Gaussian, and Laguerre-Gaussian beams: a primer," arXiv:physics/0410021 (2004).
15. A. L. F. da Silva, A. T. B. Celeste, M. Pazetti, and C. E. F. Lopes, "Formalism of operators for Laguerre-Gauss modes," arXiv: 1111.0886v1 (2011).
16. Matlab, 2015, https://uk.mathworks.com/matlabcentral/answers/179150-why-i-got-zero-answer.
17. M. R. Gleeson and J. T. Sheridan, "Non-local photo-polymerization kinetics including multiple termination mechanisms and dark reactions: part I. Modelling," J. Opt. Soc. Am. B **26**, 1736–1745 (2009).
18. S. Liu, M. R. Gleeson, D. Sabol, and J. T. Sheridan, "Extended model of the photoinitiation mechanisms in photopolymer materials," J. Appl. Phys. **106**, 104911 (2009).
19. S. Shoji, S. Kawata, A. A. Sukhorukov, and Y. Kivshar, "Self-written waveguides in photopolymerizable regins," Opt. Lett. **27**, 185–187 (2002).
20. K. Dorkenoo, A. J. van Wonderen, H. Bulou, M. Romeo, O. Crégut, and A. Fort, "Time-resolved measurement of the refractive index for photopolymerization processes," Appl. Phys. Lett. **83**, 2474–2476 (2003).
21. O. Sugihara, S. Yasuda, B. Cai, K. Komatsu, and T. Kaino, "Serially grafted polymer optical waveguides fabricated by light-induced self-written waveguide technique," Opt. Lett. **33**, 294–296 (2008).
22. K. D. Dorkenoo, F. Gillot, O. Crégut, Y. Sonnefraud, A. Fort, and H. Leblond, "Control of the refractive index in photopolymerizable materials for (2 + 1)D solitary wave guide formation," Phys. Rev. Lett. **93**, 143905 (2004).
23. Y. Qi, M. R. Gleeson, J. Guo, S. Gallego, and J. T. Sheridan, "Quantitative comparison of five different photosensitizers for use in a photopolymer," Phys. Res. Intern. **2012**, 975948 (2012).
24. E. M. Arbeloa, G. V. Porcal, S. G. Bertolotti, and C. M. Previtali, "Effect of the interface on the photophysics of Eosin-Y in reverse micelles," J. Photochem. Photobiol. A **252**, 31–36 (2013).
25. Y. Qi, H. Li, J. Guo, M. R. Gleeson, and J. T. Sheridan, "Material response of photopolymer containing four different photosensitizers," Opt. Commun. **320**, 114–124 (2014).
26. E. Tolstik, O. Romanov, V. Matusevich, A. Tolstik, and R. Kowarschik, "Formation of self-trapping waveguides in bulk PMMA media doped with phenanthrenequinone," Opt. Express **22**, 3228–3233 (2014).
27. J. R. Lawrence, F. T. O'Neill, and J. T. Sheridan, "Photopolymer holographic recording material," Optik **112**, 449–463 (2001).
28. M. R. Gleeson, S. Liu, R. R. McLeod, and J. T. Sheridan, "Non-local photo-polymerization kinetics including multiple termination mechanisms and dark reactions: part II. Experimental validation," J. Opt. Soc. Am. B **26**, 1746–1754 (2009).
29. M. R. Gleeson, S. Liu, J. Guo, and J. T. Sheridan, "Non-local photopolymerization kinetics including multiple termination mechanisms and dark reactions: part III. Primary radical generation and inhibition," J. Opt. Soc. Am. B **27**, 1804–1812 (2010).
30. J. Guo, M. R. Gleeson, S. Liu, and J. T. Sheridan, "Non-local spatial frequency response of photopolymer materials containing chain transfer agents: part I. Theoretical modeling," J. Opt. **13**, 095601 (2011).
31. G. Odian, *Principles of Polymerization*, 4th ed. (Wiley, 2004).
32. J. Guo, M. R. Gleeson, S. Liu, and J. T. Sheridan, "Non-local spatial frequency response of photopolymer materials containing chain transfer agents: part II. Experimental results," J. Opt. **13**, 095602 (2011).
33. M. R. Gleeson, J. V. Kelly, C. E. Close, F. T. O'Neill, and J. T. Sheridan, "The effects of absorption and inhibition during grating formation in photopolymer materials," J. Opt. Soc. Am. B **23**, 2079–2088 (2006).
34. M. R. Gleeson, J. V. Kelly, D. Sabol, C. E. Close, S. Liu, and J. T. Sheridan, "Modelling the photochemical effects present during holographic grating formation in photopolymer materials," J. Appl. Phys. **102**, 023108 (2007).
35. M. R. Gleeson, S. Liu, S. O'Duill, and J. T. Sheridan, "Examination of the photoinitiation processes in photopolymer materials," J. Appl. Phys. **104**, 064917 (2008).
36. S. J. Frisken, "Light-induced optical waveguide uptapers," Opt. Lett. **18**, 1035–1037 (1993).
37. J. Missinne, S. Beri, M. Dash, S. K. Samal, P. Dubruel, J. Watté, and G. V. Steenberge, "Curing kinetics of step-index and graded-index single mode polymer self-written waveguides," Opt. Mater. Express **4**, 1324–1335 (2014).
38. A. M. Ljungström and T. M. Monro, "Exploration of self-writing and photosensitivity in ion-exchanged waveguides," J. Opt. Soc. Am. B **20**, 1317–1325 (2003).
39. E. J. Galvez, *Gaussian Beams* (Colgate University, 2009).
40. P. Fulda, "Precision interferometry in a new shape: higher-order Laguerre-Gauss modes for gravitational wave detection," Doctoral thesis (University of Birmingham, 2012).
41. A. Bencheikh, M. Fromager, and K. A. Ameur, "Generation of Laguerre-Gaussian LG_{p0} beams using binary phase diffractive optical elements," Appl. Opt. **53**, 4761–4767 (2014).
42. A. Amphawan and Y. Fazea, "Laguerre-Gaussian mode division multiplexing in multimode fiber using SLMs in VCSEL arrays," J. Eur. Opt. Soc. Rapid Publ. **12**, 1–11 (2016).

43. X. Wang, Y. Liu, L. Guo, and H. Li, "Potential of vortex beams with orbital angular momentum modulation for deep-space optical communication," Opt. Eng. **53**, 056107 (2014).
44. H. Li, Y. Dong, P. Xu, Y. Qi, C. Guo, and J. T. Sheridan, "Beam self-cleanup by use of self-written waveguide generated by photopolymerization," Opt. Lett. **40**, 2981–2984 (2015).
45. M. R. Gleeson, J. T. Sheridan, F.-K. Bruder, T. Rölle, H. Berneth, M.-S. Weiser, and T. Fäcke, "Analysis of the holographic performance of a commercially available photopolymer using the NPDD model," Opt. Express **19**, 26325–26342 (2011).
46. M. B. Belgacem, S. Kamoun, M. Gargouri, K. D. Dorkenoo, A. Barsella, and L. Mager, "Light induced self-written waveguides interactions in photopolymer media," Opt. Express **23**, 20841–20848 (2015).
47. J. Guo, J. T. Sheridan, and K. Saravanamuttu, "Extremely intense filaments in large populations of self-trapped incandescent beams: spatially and temporally incoherent rogue waves," J. Opt. A **15**, 035201 (2013).
48. S. Abe and J. T. Sheridan, "Random fractional Fourier transform: stochastic perturbations along the axis of propagation," J. Opt. Soc. Am. A **16**, 1986–1991 (1999).